

# Multi-Tier Preservation of Discrete Morse-Smale Complexes in Error-Bounded Lossy Compression

Yuxiao Li , Xin Liang , Bei Wang , and Hanqi Guo 

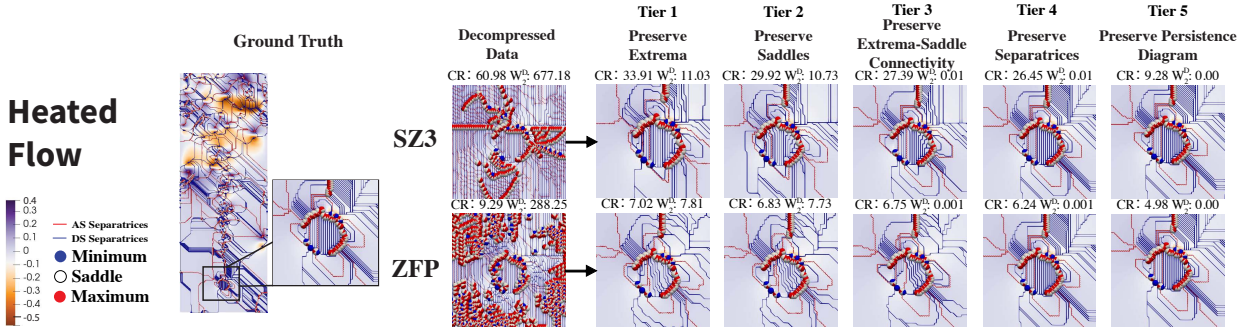


Fig. 1: Impacts of lossy compression (SZ3 and ZFP) on Morse-Smale Complexes of the Heated Flow dataset (velocity). Different tiers of topology preservation, from T1 (extrema), T2 (saddles), T3 (extrema-saddle connectivity), T4 (separatrices) to T5 (persistence diagram), are shown from left to right. CR represents the compression ratio, and  $W_2^D$  denotes the Wasserstein distance to the original data's persistence diagram.

**Abstract**— We propose a multi-tier paradigm to preserve various components of Morse-Smale complexes in lossy compressed scalar fields, including extrema, saddles, separatrices, and persistence diagrams. Existing error-bounded lossy compressors rarely consider preserving topological structures such as discrete Morse-Smale complexes, leading to significant inaccuracies in data interpretation and potentially resulting in incorrect scientific conclusions. This paper mainly focuses on preserving the Morse-Smale complexes in 2D/3D discrete scalar fields by precisely preserving critical simplices and the separatrices that connect them. Our approach generates a series of edits during compression time, which are applied to the decompressed data to accurately reconstruct the complexes while maintaining the error within prescribed bounds. We design a workflow that iteratively fixes critical simplices and separatrices in alternating steps until convergence within finite iterations. Our approach addresses diverse application needs by offering users flexible options to balance compression efficiency and feature preservation. To enable effective integration with lossy compressors, we use GPU parallelism to enhance the performance of each workflow component. We conduct experiments on various datasets to demonstrate the effectiveness of our method in accurately preserving Morse-Smale complexes.

**Index Terms**— Lossy compression, feature-preserving compression, Morse-Smale complexes.

## 1 INTRODUCTION

The rapid advancement of scientific computing and engineering simulations generates a large volume of scientific data, posing significant challenges to scientists in data storage and visualization. Error-bounded lossy compression techniques [27, 30–32, 43, 46, 47] have been widely adopted to address data challenges by achieving significant compression ratios through controlled errors in decompressed data.

However, errors introduced by the error-bounded lossy compressors may distort the topological descriptors in the decompressed data [25, 28, 45], such as Morse-Smale (MS) complexes, MS segmentations, and merge trees, affecting subsequent data analysis and leading to incorrect scientific conclusions in fields such as chemistry [4, 20], material science [19, 37], climate [11] and cosmology [40]. For example, in combustion analysis, MS complexes can be used to identify flame structures and assist scientists in understanding reaction processes, mixing, and quenching dynamics [5, 6]. Distortions in the MS complexes may lead to incorrect identification of burning zones, consequently

affecting the understanding of fuel consumption areas, as shown in Figure 2. In cosmology analysis, MS complexes can be used to identify and study the cosmic web's structure, such as filaments, walls, voids, and galaxy clusters, which are key components in the large-scale distribution of matter in the universe [42]. Distortions in the MS complexes (as shown in Figure 2) could lead to the misidentification of these structures, resulting in an incorrect understanding of matter distribution, the formation of galaxies, and the overall evolution of cosmic structures.

Preserving the MS complexes [13, 14] during data compression is particularly challenging due to their high sensitivity to tiny perturbations. These complexes consist of critical simplices (minima, saddles, maxima) and the separatrices that connect them. The construction of MS complexes relies heavily on the relative ordering of scalar values on simplices and the accurate identification of critical simplices. Consequently, even minor errors introduced by the lossy compressors can distort the topology (as shown in Figure 2), leading to unreliable identification of critical features and potentially resulting in inaccurate insights.

Preservation of MS complexes is lacking in existing lossy compression methods. While recent approaches, such as the method proposed by Li et al. [25], have attempted to preserve MS segmentation in the piecewise linear scalar field during lossy compression, they do not fully preserve the MS complexes. For example, they did not explicitly consider the preservation of saddles, which are a crucial constituent of MS complexes. Distortions in saddle points may also have a negative impact on specific applications. For example, in climate research, scientists use saddle points to identify potential turning points in storm paths [11], and inaccuracies in saddle points may lead to inaccurate

• Yuxiao Li and Hanqi Guo are with The Ohio State University. E-mail: [li.14025|guo.2154}@osu.edu](mailto:{li.14025|guo.2154}@osu.edu).  
 • Xin Liang is with the University of Kentucky. E-mail: [xliang@uky.edu](mailto:xliang@uky.edu).  
 • Bei Wang is with the University of Utah. E-mail: [beiwang@sci.utah.edu](mailto:beiwang@sci.utah.edu).

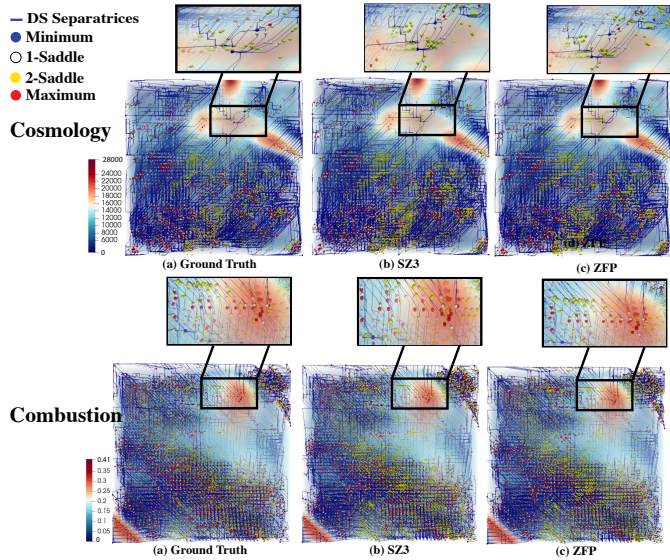


Fig. 2: Impacts of lossy compression (SZ3 and ZFP) on MS complexes under a relative error bound of  $10^{-3}$  with cosmology (top) and combustion (bottom).

weather forecasts and inadequate responses to extreme weather events.

Another observation is that different scientific applications may have varying needs for feature preservation. For example, in climate analysis, scientists may only focus on extrema to track peaks and valleys for analyzing temperature variations and cloud formation [11]. In molecular analysis, scientists often focus on the extrema of electron density, calculating various quantities to analyze molecular properties [36]. In the analysis of Atmospheric Rivers (ARs), which are extended streams of water vapor that flow from the tropics to North America and cause flooding, scientists often focus on analyzing the skeleton of ARs to better understand the formation and evolution processes [23]. In combustion analysis, saddles may be used to identify transition regions between burning cells, while the extrema-saddle connectivity can be used to understand how these cells are connected and evolve over time, and separatrices may be used to study the flow dynamics between regions [5, 6]. When dealing with noisy data, users may simplify the MS complexes based on persistence, filtering out less significant features to focus on the most critical topological structures at their desired persistence threshold.

Therefore, We propose a multi-tier topology preservation goal in lossy compression based on these varied needs to accommodate different applications' needs:

- **Tier 1 (T1): Preservation of Extrema.** This tier ensures that the **maxima** and **minima** in the decompressed data retain the same locations and types as in the original data (e.g., climate [11] and molecular analysis [36]).
- **Tier 2 (T2): Preservation of Saddles.** Building on T1, this tier ensures that the **saddles** in the decompressed data retain the same locations and types as in the original data. This further preserves all the critical simplices of the scalar field (e.g., ARs [23]).
- **Tier 3 (T3): Preservation of Extrema-Saddle Connectivity.** At this tier, the **connectivity between saddles and extrema** is preserved. Each saddle  $s_i$  must remain connected to the same maximum  $M_i$  and minimum  $m_i$  as in the original data (e.g., combustion [5, 6]).
- **Tier 4 (T4): Preservation of Separatrices.** The **separatrices** connecting saddles and extrema in the decompressed data must follow the exact same paths as in the original data, ensuring that the entire MS complex is preserved (e.g., combustion [5, 6]).
- **Tier 5 (T5): Preservation of Persistence Diagram.** The persis-

tence diagram is maintained by ensuring the filtration order is preserved. This guarantees that the simplified MS complexes at any persistence threshold are accurately preserved, with the scalar differences between connected saddles and extrema matching those in the original data (e.g., combustion [5, 6]).

Based on the multi-tier feature preservation goals outlined above, we introduce **DMTz**, a multi-tier edit-based method for preserving the discrete MS complex in 2D/3D discrete scalar fields during the compression stage of error-bounded lossy compressors by preserving all the critical simplices (including saddles) and the separatrices that connect them. The multi-tier options allow users to select the tier of topological detail most relevant to their specific applications, whether prioritizing computational efficiency or maintaining comprehensive topological information. We chose the discrete MS complex as our preservation target for its robust implementation and popular use by scientists, whereas the piecewise linear MS complex lacks a robust and open-source implementation. Our method keeps the decompressed data within the predefined error bound and could be integrated with any error-bounded lossy compressor by directly operating on the compression outputs. For a clearer comparison of the topological preservation capabilities of DMTz against other existing technologies, see Section 2.2.

We develop a workflow comprising two sub-loops: (1) the critical simplices loops (C-loops), which identify and fix false critical simplices until none remain, and (2) the separatrices loops (S-Loops), which detect and fix the inaccuracies in the separatrices. Through a finite number of iterations, the workflow identifies a subset of data that requires edits, ensuring that the MS complexes in the decompressed data remain consistent with those in the original dataset while guaranteeing the global error bound. Moreover, we enhanced the edit compression method proposed by Li et al. [25] by converting most edits into a quantized form, thereby reducing the average storage overhead required for storing the edits.

We also used GPU parallelism to accelerate each workflow component, mainly adapted from the method proposed by Li et al. [25]. Specifically, we use shared memory in our GPU implementation to efficiently extract separatrices between saddles (part of the algorithm proposed by Shivashankar et al. [39]). In summary, the contributions of this paper are multifold:

- We introduced a multi-tier feature preservation goal, surveying a wide range of scientific applications to identify the need for preserving different topological features based on different applications' needs.
- We proposed An edit-based paradigm for preserving the MS complexes within error-bounded lossy decompressed data in 2D/3D discrete scalar fields, theoretically applicable to any existing error-bounded lossy compressors.
- We improved the method for compressing the edits proposed by Li et al. [25] by converting most edits into a quantized form, resulting in an overall reduced storage overhead required for the edits.
- We conducted a comprehensive evaluation of our method using various datasets and two off-the-shelf base compressors, SZ3 and ZFP.

## 2 RELATED WORK

In this section, we review related work on error-bounded lossy compression, topology-preserving compression, and discrete MS complexes.

### 2.1 Error-Bounded Lossy Compression

Error-bounded lossy compression achieves efficient data compression while ensuring that the introduced error remains within a predefined pointwise error bound, providing high data quality. However, errors introduced by lossy compression may distort the topological descriptors in the decompressed data. Nevertheless, few error-bounded lossy compression methods consider the preservation of topological descriptors, which can impact subsequent data analysis and lead to incorrect scientific conclusions.

Error-bounded lossy compression methods can be categorized into prediction-based, transformation-based, and neural-based methods. For neural-based methods, neural networks such as autoencoders [33] and implicit neural representations [44] have been widely used for lossy data compression. Most neural compressors, though, do not ensure pointwise error control in the decompressed data. The SZ series [9, 10, 27, 30, 43, 46, 47] represents prediction-based methods that estimate data values based on neighboring information. These approaches first predict each data point using predictors like the Lorenzo predictor. The prediction residuals are then quantized and encoded using techniques such as Huffman coding, followed by lossless compression with tools like ZSTD [2] or GZIP [1]. Different from the SZ series, FPZIP [32] is another example of a prediction-based method. It reduces data size by ignoring a specified number of bit planes, while enabling on-demand control of data distortion. ISABELA [22] is another example of a prediction-based approach, utilizing B-splines to transform data points into smooth curves for prediction.

Transform-based lossy compressors convert the data into an alternative representation, such as through wavelet transforms or tensor decomposition. Once in this transformed domain, the data is compressed for significant reduction. For example, ZFP [31] transforms the data into sparse coefficients by applying a custom orthogonal block transform to decorrelate the data within blocks. These sparse coefficients are then efficiently compressed. MGARD [18] is another example of a transformation-based lossy compressor that applies wavelet theories to uniform/non-uniform structured and unstructured grids.

## 2.2 Topology Preservation in Lossy Compression

The preservation of topological structures is becoming increasingly crucial in error-bounded lossy compression. Researchers have explored various topological descriptors in both scalar and vector fields, including (1) Reeb graphs and merge/contour trees [41, 45], and (2) Morse and MS complexes [25, 26, 29]. To our knowledge, our work is the first attempt to fully preserve MS complexes.

One needs to modify the compression process to achieve topological preservation in error-bounded lossy compression. We classify these modifications into the following three categories.

**Strategy 1. Modification of compressor inputs.** Soler et al. [41] proposed TopoQZ, a topology-controlled compression method that preserves the persistence diagram by adaptively quantizing data based on a persistence simplification threshold. Their approach relies on the input of the persistence threshold for pointwise error control. In contrast, our method targets a different topological descriptor, MS complexes, and is parameter-independent.

**Strategy 2. Modification of compression algorithms.** Yan et al. [45] proposed TopoSZ, incorporating topological constraints derived from segmentations guided by contour trees by enhancing the SZ 1.4 compression algorithm. Liang et al. [26, 29] introduced cpSZ, a methodology for preserving critical points in piecewise linear and bilinear vector fields by modifying the compression algorithms. Both approaches are specific to the underlying compressor, creating a dependency on particular lossy compressors.

**Strategy 3. Modification of compression outputs.** Li et al. [25] proposed MSz, an edit-based method for preserving MS segmentations in 2D/3D piecewise linear scalar fields by focusing on extrema and the integral lines connecting them. They derive a series of edits applied to the decompressed data during compression. These edits are stored losslessly, which results in significant storage overhead. Moreover, their method does not preserve saddle points, which are crucial for the complete preservation of MS complexes. We will discuss their method in more detail in Section 3.2.

## 2.3 Morse-Smale Complexes

MS complexes, composed of critical points (maxima, minima, and saddles) and the separatrices connecting saddles to extrema, serve as fundamental topological descriptors in topological data analysis (TDA) by segmenting data into regions of uniform gradient flow, providing crucial insights into the critical features within the data. Two main approaches exist for computing MS complexes: the discrete Morse

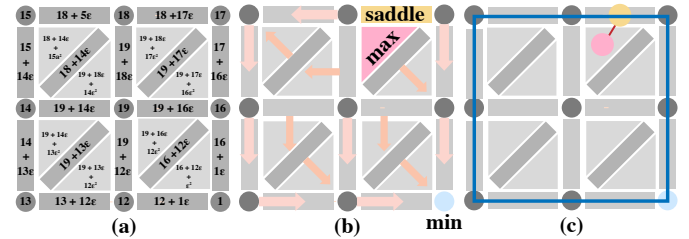


Fig. 3: (a) The discrete Morse function  $F$ , calculated by recursively extending the scalar function  $f$ , originally defined on the vertices. (b) The result of gradient pairing. Minimum(blue), saddle (yellow), and maximum (pink). (c) The discrete MS complex is extracted from (b). Ascending separatrices (red) and descending separatrices (blue).

theory [16] and the piecewise linear (PL) Morse theory [3, 14]. Each approach offers distinct advantages depending on the structure of the input data and the computational requirements; for a detailed comparison, please refer to [8].

**Discrete Morse Theory** adapts the concepts of continuous Morse theory to discrete scalar fields, enabling the computation of discrete gradient flows and the identification of critical points in grid-based data. Algorithms based on discrete Morse theory do not explicitly compute MS complexes but instead generate a discrete gradient field, from which MS complexes can be extracted as needed. Two flavors of algorithms exist for computing the discrete gradient vector field: Constrained algorithms [7, 21, 38, 39] typically start with a discrete scalar function and construct a discrete gradient field that fits the function, minimizing spurious critical simplices. Unconstrained algorithms [12, 24, 35] compute the discrete gradient field without the influence of a scalar function, often for applications in homology and persistent homology computations.

**Piecewise Linear Morse Theory** operates on continuous, triangulated domains and is primarily used for computing MS complexes from piecewise linear scalar fields defined on vertices. PL Morse theory directly computes the gradient flow and the MS complex, making it more geometrically intuitive for handling continuous spaces [3, 14].

The key difference between PL and discrete Morse theories is that PL Morse theory approximates smooth functions on triangulated surfaces. In contrast, discrete Morse theory works on cell complexes or simplicial complexes, focusing on discrete gradient flows [8].

## 3 BACKGROUND

This section reviews the background of MS complex, discrete MS complex, and feature preservation with edits in the context of lossy compression.

### 3.1 (Discrete) Morse-Smale Complexes

The discrete MS complex [17] is a discrete version of the MS complex computed using a discrete gradient vector field on a simplicial complex. A simplicial complex is a cell complex whose cells are  $d$ -dimensional simplices, where each  $d$ -simplex has exactly  $d + 1$  vertices, such as vertices (0-cells), edges (1-cells), triangles (2-cells), tetrahedra (3-cells), and so on. Our approach adopts the algorithm introduced by Shivashankar et al. [39], as its parallelization capability makes it well-suited for coupling with error-bounded lossy compressors.

The following key steps are involved in computing the discrete MS complexes: **First**, a discrete Morse function is computed by assigning values to all cells in the complex, starting from the values defined at the vertices. **Second**, the discrete gradient field is constructed by pairing cells based on their function values, which helps identify critical points. **Third**, the separatrices are extracted by tracing gradient paths between critical points, completing the domain segmentation. These steps are further detailed in the following, explaining how the discrete Morse function is constructed and how the gradient pairs are computed.

Table 1: Comparison of the Topological Preservation Capabilities between DMTz and Other Existing Techniques

Method	Data Type	Descriptor	Modification to Compression Pipeline Field	Compressor Agnostic	Extrema	Saddle	Extrema-Saddle Connectivity	Topological Segmentation	Separatrices	Persistence Diagram
DMTz (Ours)	Scalar Field	DMSC	Compression outputs (improved)	Y	Y	Y	Y	Y	Y	Y (Accurate)
MSz	Scalar Field	PLMSS	Compression outputs	Y	Y	N	N	Y	N	N
TopoSZ	Scalar Field	Contour Trees	Compression algorithm	N	Y	Y	Y	Y	N/A	N
TopoQz	Scalar Field	Contour Trees	Compression inputs	N	Y	Y	Y	Y	N/A	Y (Bounded Error)
CpSZ	Vector Field	Critical Points	Compression algorithm	N	N/A	Y	N/A	N	N	N/A

### 3.1.1 Extending Vertex Values to Discrete Morse Functions

The first step in constructing the discrete MS complex is to extend the function values from the vertices to higher-dimensional simplices. There are several approaches to generating a discrete Morse function from a scalar field. For instance, King et al. propose a method [21] that recursively extends the function from the vertices of a simplicial complex to higher-dimensional simplices. Their method focuses on reducing the number of critical points through persistence-based simplifications of critical simplices. However, the recursive nature of the algorithm and the persistence-based cancellation introduce dependencies between simplices, making this approach challenging to apply in large-scale parallel environments.

Another method introduced by Shivashankar et al. [39] recursively defines the value of the discrete Morse function on a  $d$ -dimensional simplex  $\alpha^d$ , as shown in Figure 3(a). The process starts by using the function values defined on the vertices and extends them to higher-dimensional cells, recursively defining a discrete function  $F$  on a  $d$ -dimensional simplex  $\alpha^d$  through the following equation:

$$F(\alpha^d) = F(G_0(\alpha^d)) + \varepsilon^d F(G_1(\alpha^d)) \quad (1)$$

where  $\varepsilon$  is an infinitesimally positive number used to maintain a strict ordering of function values between the cells,  $G_0(\alpha^d)$  is the face of  $\alpha^d$  with the largest function value, and  $G_1(\alpha^d)$  is the face with the largest function value among the faces that do not share vertices with  $G_0(\alpha^d)$ .

By using this equation, the order of the cells is determined by the values on their lower-dimensional faces. Instead of explicitly calculating the function values for each simplex, the algorithm only needs to compare the order of the values on the faces that make up the simplex. Since computing the MS complex requires only the relative order between cells, their method avoids explicitly calculating function values, simplifying the process and enhancing parallelizability. We chose their method because it is more suitable for parallel computation, making it easier to couple with error-bounded lossy compressors.

### 3.1.2 Extracting Critical Simplices

Once the discrete Morse function is computed, the discrete gradient is constructed by pairing all cells in the simplicial complex. For each  $d$ -simplex  $\alpha^d$ , the discrete gradient pairs it with a  $(d+1)$ -simplex  $\beta^{d+1}$ , provided  $\alpha^d$  is the face with the highest function value in  $\beta^{d+1}$ , as shown in Figure 3(b). To determine the pairing, we:

- Find all cofacets  $\beta^{d+1}$  of a given simplex  $\alpha^d$ , where  $\alpha^d$  is the face with the highest scalar value.
- Pair  $\alpha^d$  with the cofacet  $\beta^{d+1}$  that has the smallest function value.

Cells that are not paired in this process are critical cells. For example, in 2D, unpaired vertices are minima, unpaired edges are saddles, and unpaired faces are maxima. In 3D, the classification includes 1-saddles (unpaired edges) and 2-saddles (unpaired faces).

### 3.1.3 Connecting Critical Simplices

The discrete MS complex is extracted by tracing gradient paths formed by the computed gradient pairs, as shown in Figure 3(c). A gradient path is a sequence of cells connected by their discrete gradient, and it traces the flow of scalar values from one critical point to another (e.g., from a saddle to a maximum or minimum).

By following these paths, we can extract the separatrices that connect critical points, segmenting the domain based on the scalar field's topology. In 2D, minima connect to saddles, and saddles connect to maxima. In 3D, minima connect to 1-saddles, 1-saddles connect to 2-saddles, and 2-saddles connect to maxima.

### 3.1.4 Generating Persistence Diagram through Filtration

Researchers often use persistence diagrams [15] to simplify the MS complex by removing low-persistence features regarded as noise.

After computing the discrete MS complex, topological features are analyzed using filtration, which is constructed by gradually increasing a scalar threshold. As the scalar threshold increases, topological features such as connected components, loops, and cavities appear (birth, usually at minima) and disappear (death, often at saddles or maxima) across multiple scales. By tracking pairs of critical points, a persistence diagram is generated. This diagram captures the scalar value differences between critical points, representing the duration of features—longer persistence indicates more significant features, while shorter persistence indicates noise.

## 3.2 Edit-based Strategy for Feature Preserving Compression

We have adopted and improved upon the edit-based feature preservation method in error-bounded lossy compressors proposed by Li et al. [25]. Their approach primarily involves deriving a series of edits through a finite number of iterations during the compression process. These edits are then applied to the decompressed data to accurately reconstruct the features that need to be preserved while ensuring the error remains within the prescribed bound.

Since the edits are directly applied to the decompressed data, this method can be applied to any existing error-bounded lossy compressor without being tied to the specific compression algorithm. However, introducing these edits does come with some storage overhead, as the edits need to be stored along with the compressed data. We have improved their method of storing edits, which resulted in an overall decrease in storage overhead.

The general approach involves identifying distorted features during each iteration and modifying the scalar value of specific data points to correct these distortions. However, the modification may introduce new distortions, leading to further iterations. The process continues until all targeted features are accurately preserved, at which point the iterations exist.

The key to the convergence of the iterative process is that the edits applied to each data point are either negative or zero. Specifically, for a data point  $i$  at iteration  $k$ , the edited scalar value  $g_i^{(k)}$  satisfies:

$$\hat{f}_i = g_i^{(0)} \geq \dots \geq g_i^{(k)} \geq g_i^{(k+1)} \geq \dots > f_i - \xi, \quad (2)$$

where  $\hat{f}_i$  is the initial decompressed value. Since the original data has an inherent order, and the edits on data point  $i$  are always negative or zero, one can always find a finite iteration  $k$  where the scalar value of  $i$  and its neighbors align with the original data's order. In the worst case, all data points decrease to the lower bound  $f_i - \xi$ , and the order of all points will match that of the original data, ensuring that the iterations converge.

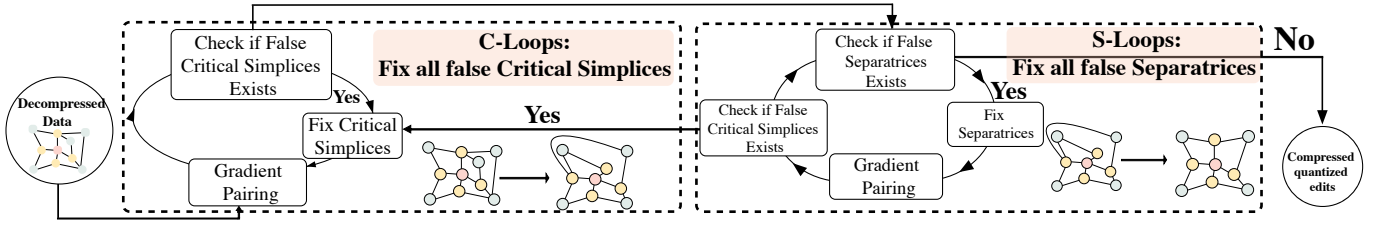


Fig. 4: An illustration of the workflow of our algorithm for preserving the full MS complexes. Our algorithm gets a series of edits during the compression time with two distinct loops: (1) C-Loops, which iteratively fix all false critical simplices, and (2) S-Loops, which iteratively fix all false separatrices. The C-Loops and S-Loops alternate until no false critical simplices or separatrices exist. The quantized edits are losslessly compressed and included with the compressed data in the compression output. The edits are applied to the decompressed data to correct MS complexes in the decompression stage.

## 4 PROBLEM STATEMENT AND METHODOLOGY

### 4.1 Problem Statement

We now formulate the preservation of different tiers of features within MS complexes in 2D and 3D discrete scalar fields. Each tier is designed to preserve specific features, from extrema to persistence diagram, ensuring that the decompressed data retains its topological integrity across varying tiers of detail. Regardless of the tier, we also need to preserve the global error bound. We must ensure the pointwise error between the edited decompressed data and the original data remains within the predefined error bound. That is, for any vertex  $i$ ,  $|g_i - f_i| \leq \xi$ . For the specific objectives of feature preservation for each tier, please refer to Section 1.

### 4.2 Methodology

To achieve the preservation goals as formulated above, our method addresses distortions in critical simplices or separatrices. Distortions in critical simplices or separatrices are caused by incorrect gradient pairing results based on comparing the function values of simplices with their faces and cofaces. These function values are extended from the scalar values of the vertices, as derived through Equation 1. Therefore, we can correct the gradient pairing results by editing the scalar values of the vertices.

Without loss of generality, our method identifies a vertex  $v$  among the vertices that constitute the false critical simplex or the *troublemaker* (defined as the first simplex along the separatrices where the gradient pairing is incorrect) and their neighboring vertices, then reduces its value using the following equation.

$$g_v^{(k+1)} := \begin{cases} g_v^{(k)} - \frac{\xi}{2^{h+1}}, & \text{if } h < q, \\ f_v - \xi, & \text{if } h \geq q \end{cases} \quad (3)$$

where  $g_v^{(k)}$  is the edited value at  $v$  during the  $k$ th iteration,  $h$  is the number of times  $v$  has been edited, and  $q$  is a user-defined hyperparameter. Once a vertex  $v$  has been edited  $q$  times, its edited value is directly set to  $f_v - \xi$ , and  $\delta_v$  is stored losslessly.

Specifically, we design a theoretical workflow for obtaining the vertex-wise edits during the compression time (see Figure 4). Our workflow operates through alternating iterations of two main loops: (1) the Critical Simplices Loops (C-Loops) and (2) the Separatrices Loops (S-Loops).

C-Loops preserve the extrema (T1) and saddles (T2, T3, T4, T5), while S-Loops preserve the connectivity (T3) or separatrices (T4, T5) among saddles and extrema.

The notations used throughout our paper are as follows:  $\xi$  represents the global error bound, and  $v_i$  denotes the  $i$ -th vertex.  $e_{ij}$  refers to the edge consisting of vertices  $v_i$  and  $v_j$ , while  $t_{ijk}$  denotes the triangle formed by  $v_i$ ,  $v_j$ , and  $v_k$ , and  $d_{ijk}$  represents the tetrahedron consisting of vertices  $v_i$ ,  $v_j$ ,  $v_k$ , and  $v_m$ . The scalar values at vertex  $v_i$  in the original and decompressed data are represented by  $f_i$  and  $\hat{f}_i$ , respectively, while  $g_i$  refers to the edited scalar value at  $v_i$ , and  $P_i$  denotes the set  $P_\alpha$  associated with a simplex  $i$ .

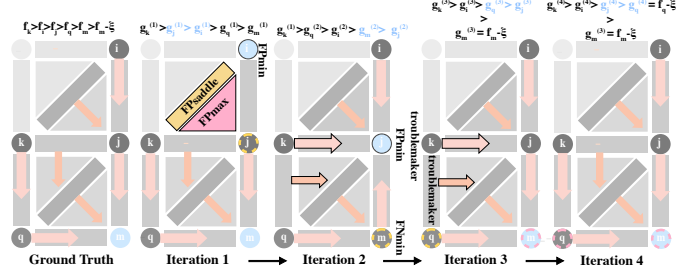


Fig. 5: Fixing FPmin, FPmax, FNmin (and subsequently, another FPmin, FNmin, and two troublemakers) across C- and S-Loops. Cells with black outlines represent false cases, vertices with yellow dashed outlines indicate the vertex to be edited in the current iteration, and those with pink dashed outlines signify vertices whose values have already been set to the lower bound. The values above represent the scalar value relationships between vertices in each iteration, with the blue highlights marking the incorrect relationships.

### 4.3 Critical Simplices Loops (C-Loops)

The C-Loops (as shown in Algorithm 1) focus on fixing all false critical simplices, including false positive/negative minima, saddles, and maxima. False positive cases are defined as simplices paired with their face/cofacet in the original data but not paired with any in the decompressed data. Conversely, false negative cases are simplices that were unpaired in the original data but paired with one of their faces/cofacets in the decompressed data.

We will discuss the method for selecting the vertex  $v$  that needs editing in different cases below and use Figure 5 to explain the process. **False Positive Minimum (FPmin)** in both 2D and 3D cases are represented by vertices. Let  $e_{ij} = (v_i, v_j)$  represent the edge paired with an FPmin  $v_i$  in the original data, and  $g_i^{(k)}$  is the edited value at  $i$  during the  $k$ th iteration.

In Figure 5(b),  $v_i$  is an FPmin. In the original data,  $v_i$  is paired with  $e_{ij}$  because  $f_i > f_j$ . However, in the decompressed data,  $g_i^{(1)} < g_j^{(1)}$ , preventing  $v_i$  from being correctly paired, which causes it to become an FPmin. In this case, we decrease the value of  $v_j$  using Equation 3 so that the scalar relationship between  $v_i$  and  $v_j$  is corrected, allowing  $v_i$  to be correctly paired with  $e_{ij}$ .

**False Negative Minimum (FNmin)** could be fixed by decreasing the value of itself. In Figure 5 (c), the FNmin  $v_m$  is incorrectly paired with  $e_{jm} = (v_j, v_m)$  because  $g_m^{(2)} > g_j^{(2)}$ , we reducing  $g_m^{(2)}$  so that  $v_m$  will no longer pair with any edge, and it will instead become a minimum.

**False Positive 1-Saddle (FP1saddle)** should be paired with a vertex/triangle in the original data. For example, in Figure 5,  $e_{ik}$  is paired with  $t_{ijk}$  in the original data, which implies that  $f_k > f_j$  and  $f_i > f_j$ . However, in the decompressed data,  $g_j^{(2)} > g_i^{(2)}$ , making  $e_{ik}$  unpaired. In this case, we reduce the value of  $v_j$  to ensure that  $e_{ik}$  is correctly

paired again. Cases where  $e_{ik}$  is paired with a vertex are handled similarly. Generally, we determine which vertex  $v$  needs to be edited using the following equation.

$$v := \begin{cases} v \in e_{ik} \text{ and } v \neq v_i, & \text{if } e_{ik} \text{ is paired with } v_i \text{ in } f, \\ v \in t_{ijk} \text{ and } v \notin e_{ik}, & \text{if } e_{ik} \text{ is paired with } t_{ijk} \text{ in } f. \end{cases} \quad (4)$$

**False Negative 1-Saddle (FN1saddle)** could be fixed by making it unpaired in the decompressed data. If an FN1saddle  $e_{ij}$  is paired with  $v_i$  in the decompressed data, we need to reduce the value of  $v_i$  so that  $g_i < g_j$ , preventing  $e_{ij}$  from pairing with  $v_i$ . Similarly, if it is paired with  $t_{ijk}$ , we reduce the value of either  $v_i$  or  $v_j$ , ensuring that  $e_{ij}$  cannot pair with  $t_{ijk}$ . We determine which vertex  $v$  needs to be edited by the following equation:

$$v := \begin{cases} v_i, & \text{if } e_{ij} \text{ is paired with } v_i \text{ in } \hat{f}, \\ \arg \max_{v \in e_{ij}} F(v), & \text{if } e_{ij} \text{ is paired with } t_{ijk} \text{ in } \hat{f}. \end{cases} \quad (5)$$

**False Positive 2-Saddle (FP2saddle)** only exist in 3D, and the solution to fix an FP2saddle  $t_{ijk}$  is similar to FP1Saddle. We decrease the value of  $v$ , where  $v$  is chose by the following equation:

$$v := \begin{cases} v \in t_{ijk} \text{ and } v \notin e_{ij}, & \text{if } t_{ijk} \text{ is paired with } e_{ij} \text{ in } f, \\ v \in d_{ijkm} \text{ and } v \notin t_i, & \text{if } t_{ijk} \text{ is paired with } d_{ijkm} \text{ in } f. \end{cases} \quad (6)$$

**False Negative 2-Saddle (FN2saddle)** can be fixed using a similar solution as that for FN1saddles. We decrease the value of  $v$  to fix an FN2saddle  $t_{ijk}$ , where  $v$  is chose by the following equation:

$$v := \begin{cases} \arg \max_{v \in e_{ij}} F(v), & \text{if } t_{ijk} \text{ is paired with } e_{ij} \text{ in } \hat{f}, \\ \arg \max_{v \in t_{ijk}} F(v), & \text{if } t_{ijk} \text{ is paired with } d_{ijkm} \text{ in } \hat{f}. \end{cases} \quad (7)$$

**False Positive Maximum (FPmax)** in 2D, maxima is represented by a triangle, while in 3D, it is represented by a tetrahedron. Therefore, we discuss these cases separately: **Case I**: In a 2D case, as shown in Figure 5 (b), triangle  $t_{ijk}$  is an FPmax which should paired with  $e_{ik}$  in the original data. We then decrease the value of  $v$  so that we can correct the gradient pairing result for  $t_{ijk}$ . **Case II**: In a 3D case, the FPmax is a tetrahedron  $d_{ijkm}$ . Assuming that  $d_{ijkm}$  is paired with a triangle  $t_{ijk}$  in the original data. Similarly, we then decrease the value of  $v$ , where  $v \in d_{ijkm}$  and  $v \notin t_{ijk}$ .

**False Negative Maximum (FNmax)** could also be divided into two cases: **Case I**: In a 2D case, the FNmax is a triangle  $t_{ijk}$ . Assuming that  $t_{ijk}$  is paired with an edge  $e_{ij}$  in the decompressed data. We then decrease the value of  $v$ , where  $v = \arg \max_{v \in e_{ij}} F(v)$ . **Case II**: In a 3D case, the FNmax is a tetrahedron  $d_{ijkm}$ . Assuming that  $d_{ijkm}$  is paired with a triangle  $t_{ijk}$  in the decompressed data. We then decrease the value of  $v$ , where  $v = \arg \max_{v \in t_{ijk}} F(v)$ .

#### 4.4 Separatrices loops (S-Loops)

After all false critical simplices are fixed, our next step is to fix any incorrect gradient pairs encountered while tracing the separatrices from each saddle based on the gradient pairing results. This ensures the complete preservation of the separatrices connecting critical simplices.

For any incorrect critical pair, our method involves three key steps in each iteration: (1) compute the ascending and descending paths in the currently edited data  $g^{(k)}$  based on the gradient pairing results of each saddle's face/cofacet, (2) identify the *troublemaker* (3) editing the scalar value of the vertices that form the *troublemaker* to correct the gradient pairing results.

In Figure 5(d),  $v_k$  and  $e_{kq}$  are both troublemakers and paired with each other in the original data, but they are paired with other simplices in the decompressed data. Therefore, we reduce the value of  $v_q$  to correct their gradient pairing result. Generally, given a troublemaker, assume that in the edited data  $g^{(k)}$ , the troublemaker is paired with simplex  $i$ , while in the original data, it is paired with simplex  $j$ . Then, we decrease the value of  $v$ , where  $v \in$  simplex  $i$  and  $v \notin$  simplex  $j$ .

After the S-Loops are completed, modifications to the data may introduce new false critical points. Therefore, we must execute the

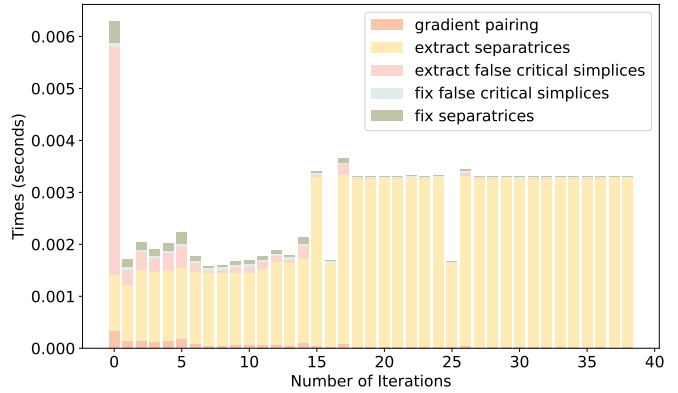


Fig. 6: Timings of different components per iteration.

C-Loops again to correct these false cases. This requires us to alternate between the C- and S-Loops until all false critical simplices and inaccurate separatrices are eliminated. For the proof of convergence for this alternating process, see Section 3.2.

#### 4.5 Quantized Representation of Edits

We improved the lossless compression method used by Li et al. [25] (referred to as floating edits in the following), which directly compressed the edits  $\delta_i$  as floating-point numbers in a key-value pair format. Their method requires significant storage overhead for the floating-point representations, mainly when dealing with large datasets or frequent edits, which can lead to inefficiencies in compression.

In our method, each edit  $\delta_i$  is quantizable as it is determined by Equation 3 (referred to as discrete edits in the following), which ensures that if a vertex  $v_i$  is edited  $m$  times, then  $\delta_i$  can be expressed as:

$$\delta_i = \frac{\xi}{2} + \frac{\xi}{2^2} + \dots + \frac{\xi}{2^m} = \xi \left(1 - \frac{1}{2^m}\right). \quad (8)$$

By storing only the value of  $m$ , which can be efficiently represented using a limited number of bits, we can efficiently reconstruct the exact delta value  $\delta_i$  without storing multiple floating-point numbers. This quantization approach may significantly reduce the storage overhead associated with edits, particularly when  $m$  values are small or constrained within a limited range.

Furthermore, to handle cases where the number of edits for a vertex  $v_i$  exceeds the user-defined hyperparameter  $q$ , we store the edited  $v_i$  directly as  $f_i - \xi$  in a lossless format. Given that such cases are relatively sparse (as shown in Figure 9), this approach could effectively reduce the amount of floating-point data requiring lossless storage, thereby improving the overall compression ratio.

#### Algorithm 1 C-Loops

```

Input: original data  $f$ , current decompressed data  $\hat{f}$ , error bound  $\xi$ , original gradient pairing result  $G_o$ 
 $G_d \leftarrow \text{gradient\_pairing}(\hat{f})$ 
 $\text{false\_criticals} \leftarrow \text{extract\_false\_critical\_simplices}(G_o, G_d)$ 
while  $\text{false critical simplices}$  exits do
  for each  $\alpha \in \text{false\_criticals}$  do
     $\text{fix\_false\_criticals}(\alpha)$ 
  end for
   $G_d \leftarrow \text{gradient\_pairing}(\hat{f})$ 
   $\text{false\_criticals} \leftarrow \text{extract\_false\_critical\_simplices}(G_o, G_d)$ 
end while

```

#### 4.6 Multi-Tier Preservation

We designed our method to support multiple tiers of topological feature preservation because different applications may have varying requirements for preserving topological structures. For example, in climate

analysis, scientists may only need to preserve extrema (T1) to track peaks and valleys to analyze temperature variations and cloud formation [11]. In such cases, preserving all the details of the MS complex would lead to unnecessary computational and storage overhead.

For instance, preserving the connections between 1-saddles and 2-saddles is particularly challenging due to the complexity of 1-saddle-2-saddle gradient paths [39]. These paths can merge or split, making the preservation process highly intricate. Even minor errors in these connections can lead to significant distortions, requiring numerous iterations to correct. As a result, a substantial amount of time may be spent extracting and fixing saddle-to-saddle connectors, as shown in Figure 6, which may not be necessary for specific applications.

To address this variability, we allow users to choose the tier of topological detail they need to preserve (as shown in Figure 1). For example, in T2, only the C-Loops are necessary to fix all false critical simplices, and the process completes without requiring the execution of S-Loops.

## 5 EVALUATION

We evaluate our method using datasets from various fields, including climate, combustion, cosmology, molecular dynamics, and so on. To get the decompressed data, we selected two state-of-the-art error-bounded lossy compressors, SZ3 and ZFP, as our base compressors. Evaluation metrics are as follows: **Overall Compression Ratio (OCR)** is the compression ratio after combining the compressed edits, calculated by the combined size of compressed edits and data over the original data size. **Edit ratio** quantifies the proportion of edited data points to fully preserve the MS complex in the decompressed data. It is calculated as the number of modified data points divided by the total number of data points. **Overall bit rate (OBR)** represents the average number of bits required to encode each data point after compression (after the combination of compressed edits). It is calculated by dividing the total number of bits used by the total number of data points. Lower bit rates indicate more efficient compression. **PSNR distortion** describes the relationship between the bitrate and PSNR. It illustrates how changes in bitrate impact the PSNR, with higher bitrates typically leading to higher PSNR, indicating better data quality. This relationship is usually depicted as a curve, where the x-axis represents the bitrate, and the y-axis represents the PSNR of the decompressed data.

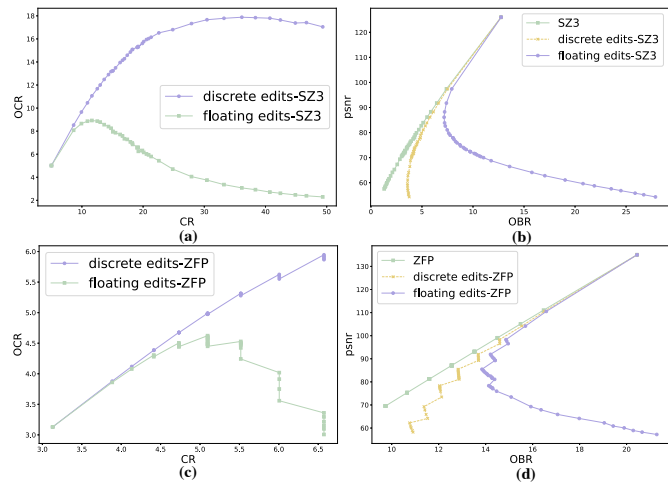


Fig. 7: Storage overhead caused by the edits on CESM dataset using: (a) and (b): SZ3; (c) and (d): ZFP.

### 5.1 Multitier Preservation Comparison

We evaluated our methods for preserving MS complexes on both the Heated Flow and the Integrated Vapor Transport (IVT) datasets under different tiers of preservation. For the Heated Flow dataset, we cropped a specific region to better visualize the differences between the decompressed and original data, which were quantified using the Wasserstein

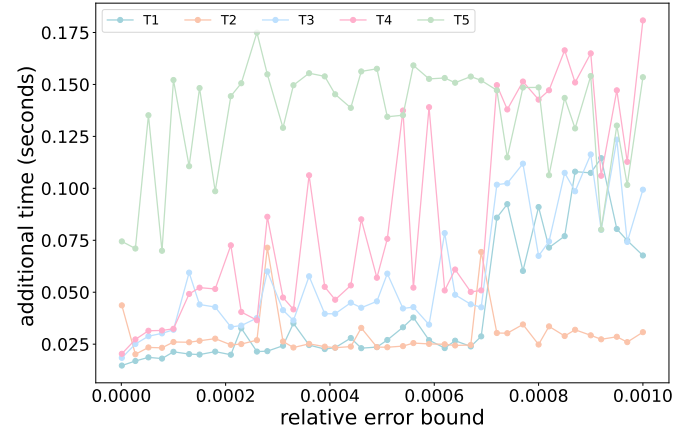


Fig. 8: Timings of computation overhead of different tiers of preservation on the IVT dataset using SZ3 ranging from: T1 (blue), T2 (orange), T3 (green), T4 (pink), to T5 (light green).

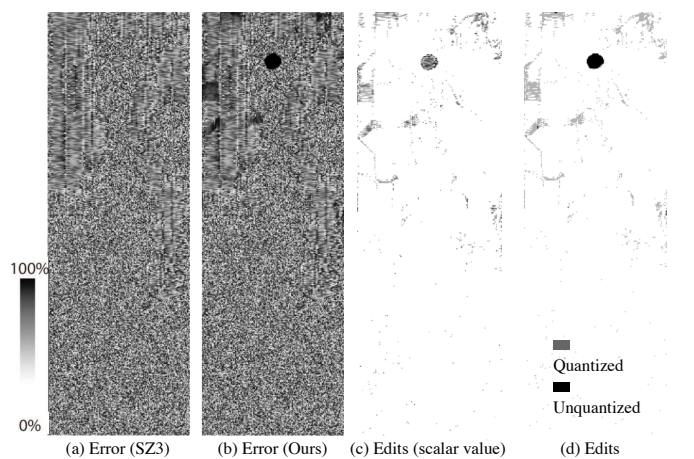


Fig. 9: Error distribution of (a) SZ3 and (b) ours (SZ3); edit distribution represented by (c) scalar values and (d) gray blocks for quantized edits and black blocks for unquantized edits.

distance ( $W_2^D$ ) between their persistence diagrams, as shown in Figure 1. The initial decompressed data from both SZ3 and ZFP showed varying degrees of distortion in the MS complexes, with initial Wasserstein distances ( $W_2^D = 688$  for SZ3 and  $W_2^D = 288$  for ZFP) indicating significant topological distortions.

For the IVT dataset, we conducted a series of experiments with various error bounds to compare the computation overhead across different tiers of preservation. The results (as shown in Figure 8) showed that the computation overhead increased roughly proportionally with the tier of preservation, following the magnitude of the global error bound. In both datasets, the computation and storage overheads increased roughly proportionally with higher preservation requirements. This trend is reasonable, as finer preservation of topological structures leads to a lower tolerance for errors in the data, necessitating more edits and iterations.

### 5.2 Compression of Edits

We compare the storage overhead of our approach for lossless compression of edits with the method proposed by Li et al. [25] when fully preserving the MS complexes on the CESM dataset. We run an ensemble of experiments with various error bounds ranging from  $10^{-6}$  to  $10^{-3}$  as shown in Figure 7.

We observed that our method improves the overall compression ratio compared to the method by Li et al., with up to 6 times higher for SZ3 and up to 2 times higher for ZFP, on average. This improvement

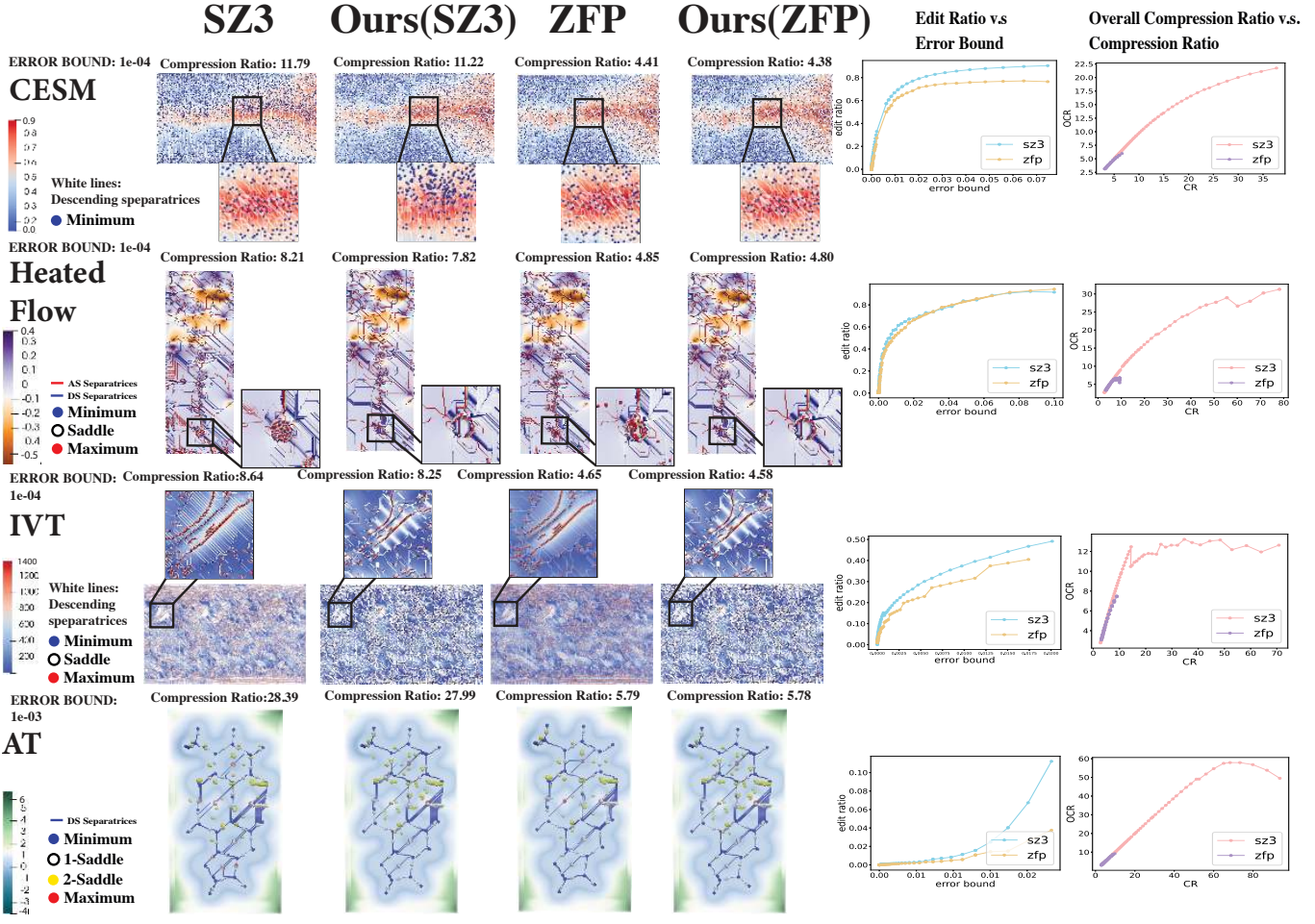


Fig. 10: Comparison of the capabilities of different lossy compressors to preserve MS complexes on fixed error bound across different datasets.

Dataset	Dimensions	Ours-SZ ( $10^{-5}$ )			Ours-ZFP ( $10^{-5}$ )			Ours-SZ ( $5 \times 10^{-5}$ )			Ours-ZFP ( $5 \times 10^{-5}$ )			GZIP		ZSTD	
		$t_{comp}$	$t_{fix}$	OCR	$t_{comp}$	$t_{fix}$	OCR	$t_{comp}$	$t_{fix}$	OCR	$t_{comp}$	$t_{fix}$	OCR	$t_{comp}$	CR	$t_{comp}$	CR
AT	$177 \times 95 \times 48$	0.19	2.23	7.07	0.19	0.69	3.75	0.25	4.52	10.71	0.39	0.69	4.25	0.24	1.07	1.18	1.17
IVT	$361 \times 576$	0.25	0.05	5.31	0.70	0.04	3.80	0.15	0.05	7.08	0.40	0.07	4.34	0.07	1.06	0.02	1.10
Heated Flow	$150 \times 450$	0.08	0.02	4.27	0.11	0.02	3.97	0.08	0.04	6.52	0.10	0.03	4.49	0.64	1.91	1.21	2.00
CESM-ATM	$1800 \times 3600$	0.84	2.98	7.32	1.71	1.84	3.66	0.78	5.86	9.59	0.63	3.23	4.11	3.37	2.08	1.65	2.27

Table 2: Compression time and compression ratios in Ours-SZ, Ours-ZFP, two lossless compressors: GZIP, and ZSTD.  $t_{comp}$  and  $t_{fix}$ , respectively, represent the timings (in seconds) of the base compressors and our algorithm.

generally becomes more significant as the original compression ratio increases; that is, higher original compression ratios lead to greater relative enhancement by our method.

This trend can be attributed to the fact that higher compression ratios in lossy compression will introduce more errors in the decompressed data, necessitating a greater number of edits to preserve the MS complexes accurately. By effectively quantizing many of these edits, our method allows for more efficient lossless compression compared to the original edits compression method. Additionally, as shown in Figure 9, the edits that need to be stored in a lossless format in our method are relatively sparse distributed, further contributing to the improved compression ratio.

### 5.3 Feature Preservation across Error Bounds

We demonstrate the ability of our method to fully preserve the MS complexes with different compressors and error bounds across various datasets while maintaining acceptable storage overhead, as shown in Figure 10. Consistent with the discussion in Section 5.2, the number of edits generally shows a proportional relationship with the error bounds.

We also observed that the number of required edits increases with the complexity of the dataset; for instance, the average edit ratio is lower for the AT dataset compared to the CESM, Heated Flow, and IVT datasets.

Furthermore, the number of edits required by ZFP is generally lower than for SZ3, and ZFP's overall compression ratio is also lower than SZ3. This is because ZFP's original compression ratio is typically lower than SZ3, which introduces fewer errors in the decompressed data, resulting in less distortion in the MS complexes and requiring fewer edits. We also observe a trade-off between the error bound and the preservation of MS complexes, where a higher error bound results in larger pointwise errors between the decompressed and original data, causing more severe distortion of the MS complexes.

### 5.4 Feature Preservation across Bit Rates

We evaluated our method for preserving MS complexes by determining the achievable optimal overall bit rate. We conducted a series of experiments with various error bounds on SZ3 and ZFP, finding the closest bit rate to assess the ability to preserve MS complexes in the decom-

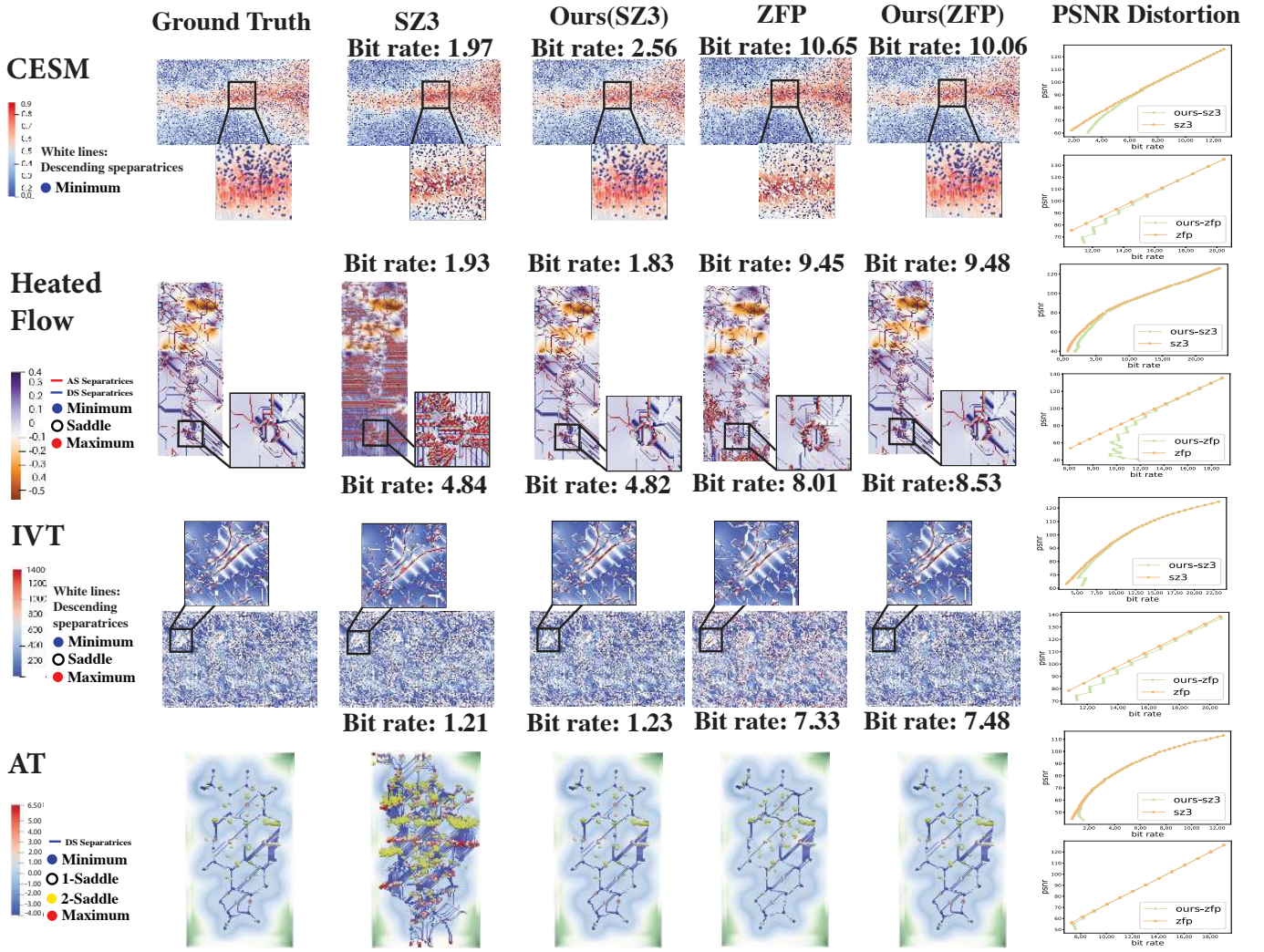


Fig. 11: Comparison of the capabilities of different lossy compressors to preserve MS complexes on fixed bit rate across different datasets.

pressed data. At similar bit rates, both SZ3 and ZFP’s decompressed data exhibited varying degrees of MS complex distortion, particularly in the AT dataset, where significant distortion was observed at a bit rate of 1.21 for SZ3. Additionally, we found that the optimal bit rate achieved by ZFP was approximately 4 times higher than that of SZ3 across all datasets, which could be attributed to ZFP’s inherently higher original bit rate.

## 6 DISCUSSION AND LIMITATION

### 6.1 Computational and Storage Overhead

The computation of MS complexes is an essential step in our method, while the efficient computation of MS complexes is already a known challenge [34], particularly for extracting separatrices. Users may adjust the tier of topology preservation based on their specific requirements and available computational resources, balancing the trade-off between the accuracy of MS complexes and the performance.

We compared the computational overhead introduced by our method on SZ3 and ZFP in various datasets with GZIP and ZSTD, as shown in Table 2. GZIP and ZSTD generally achieve a compression ratio of around 2.0, while our method consistently surpasses this with an average compression ratio above 2.0. Although our approach introduces a tolerable computation overhead on the scale of seconds, it still preserves the MS complexes.

One limitation of our method is that it is tailored to the approach by Shivashankar et al. [39] for extracting MS complexes, so it inherits

some drawbacks. For instance, their method can introduce many low-persistence critical points in noisy data, necessitating additional edits in our approach and leading to increased storage overhead.

### 6.2 Preservation of Simplified Morse-Smale complexes

Our method could preserve the persistence diagram, which allows for the preservation of simplified MS complexes at any given persistence threshold. However, preserving a specific simplified MS complex is non-trivial. First, the simplification of MS complexes is time-consuming, as it requires calculating the full MS complex before deriving the simplified version. Our algorithm necessitates recalculating the simplified MS complex of the decompressed data in each iteration, which may significantly increase the computation overhead. Second, this simplification alters the gradient pairing results, which are critical for our approach in correcting false critical points and separatrices. As a result, any changes introduced during the simplification process could interfere with the subsequent steps.

## 7 CONCLUSIONS AND FUTURE WORK

We presented a multi-tier approach for preserving key topological features of MS complexes in error-bounded lossy compression. By allowing tiered preservation of extrema, saddles, separatrices, and persistence diagrams, our method offers users flexible options to balance compression efficiency and feature preservation. Additionally, we incorporate parallelism to accelerate the workflow components. We

demonstrate our method's capability to preserve the MS complexes in 2D/3D discrete scalar fields across various datasets and tiers.

We plan to improve our method in various aspects. First, we will focus on preserving simplified MS complexes under a specific persistence threshold; addressing the time-consuming simplification process, recalculating the simplified complex iteratively, and managing the gradient pairing modifications caused by simplification will be key areas of exploration. Second, we plan to extend our method to better handle noisy data by integrating more robust noise filtering techniques, such as persistence-based simplification, reducing the impact of low-persistence critical points on computational and storage overhead.

## ACKNOWLEDGMENTS

This research is supported by the U.S. Department of Energy, Office of Advanced Scientific Computing Research (DE-SC0022753, DE-SC0021015) and the National Science Foundation (OAC-2311878, OAC-2313123, OAC-2313124, IIS-1955764, OAC-2330367, OAC-2313122, and OIA-2327266). This research used resources of the National Energy Research Scientific Computing Center (NERSC), a Department of Energy Office of Science User Facility.

## REFERENCES

- [1] GZIP. <https://www.gzip.org/>. Accessed: September 20, 2024. 3
- [2] ZSTD. <http://www.zstd.net>. Accessed: September 20, 2024. 3
- [3] T. Banchoff. Critical points and curvature for embedded polyhedra. *Journal of Differential Geometry*, 1(3-4):245–256, 1967. doi: 10.4310/jdg/1214428092 3
- [4] H. Bhatia, A. G. Gyulassy, V. Lordi, J. E. Pask, V. Pascucci, and P.-T. Bremer. Tms: Comprehensive topological exploration for molecular and condensed-matter systems. *Journal of Computational Chemistry*, 39(16):936–952, 2018. doi: 10.1002/jcc.25181 1
- [5] P.-T. Bremer, G. Weber, V. Pascucci, M. Day, and J. Bell. Analyzing and tracking burning structures in lean premixed hydrogen flames. *IEEE Transactions on Visualization and Computer Graphics*, 16(2):248–260, 2010. doi: 10.1109/TVCG.2009.69 1, 2
- [6] P.-T. Bremer, G. Weber, J. Tierny, V. Pascucci, M. Day, and J. Bell. Interactive exploration and analysis of large-scale simulations using topology-based data segmentation. *IEEE Transactions on Visualization and Computer Graphics*, 17(9):1307–1324, 2011. doi: 10.1109/TVCG.2010.253 1, 2
- [7] F. Cazals, F. Chazal, and T. Lewiner. Molecular shape analysis based upon the Morse-Smale complex and the connolly function. In *Proceedings of the Nineteenth Annual Symposium on Computational Geometry*, SCG '03, 10 pages, p. 351–360. Association for Computing Machinery, New York, NY, USA, 2003. doi: 10.1145/77792.777845 3
- [8] L. De Floriani, U. Fugacci, F. Iuricich, and P. Magillo. Morse complexes for shape segmentation and homological analysis: discrete models and algorithms. *Computer Graphics Forum*, 34(2):761–785, 2015. doi: 10.1111/cgf.12596 3
- [9] S. Di and F. Cappello. Fast error-bounded lossy HPC data compression with SZ. In *Proceedings of IPDPS'16: Proceedings of the 2016 IEEE International Parallel and Distributed Processing Symposium*, pp. 730–739, 2016. doi: 10.1109/IPDPS.2016.111 3
- [10] S. Di and F. Cappello. Optimization of error-bounded lossy compression for hard-to-compress HPC data. *IEEE Transactions on Parallel and Distributed Systems*, 29(1):129–143, 2018. doi: 10.1109/TPDS.2017.2749300 3
- [11] H. Doraiswamy, V. Natarajan, and R. S. Nanjundiah. An exploration framework to identify and track movement of cloud systems. *IEEE Transactions on Visualization and Computer Graphics*, 19(12):2896–2905, 2013. doi: 10.1109/TVCG.2013.131 1, 2, 7
- [12] P. Dłotko, T. Kaczynski, M. Mrozek, and T. Wanner. Coreduction homology algorithm for regular cw-complexes. *Discrete & Computational Geometry*, 46:361–388, 2011. 3
- [13] H. Edelsbrunner, J. Harer, V. Natarajan, and V. Pascucci. Morse-Smale Complexes for piecewise linear 3-manifolds. In *Proceedings of the Nineteenth Annual Symposium on Computational Geometry*, SCG '03, 10 pages, pp. 361–370, 2003. doi: 10.1145/77792.777846 1
- [14] H. Edelsbrunner, J. Harer, and A. Zomorodian. Hierarchical Morse complexes for piecewise linear 2-manifolds. In *Proceedings of the Seventeenth Annual Symposium on Computational Geometry*, 10 pages, pp. 70–79, 2001. doi: 10.1145/378583.378626 1, 3
- [15] H. Edelsbrunner, D. Letscher, and A. Zomorodian. Topological persistence and simplification. In *Proceedings of 41st Annual Symposium on Foundations of Computer Science*, pp. 454–463, 2000. doi: 10.1109/SFCS.2000.892133 4
- [16] R. Forman. Morse theory for cell complexes. *Advances in Mathematics*, 134(1):90–145, 1998. doi: 10.1006/aima.1997.1650 3
- [17] R. Forman. A user's guide to discrete Morse theory. *Sém. Lothar. Combin.*, 48, 12 2001. 3
- [18] Q. Gong, J. Chen, B. Whitney, X. Liang, V. Reshniak, T. Banerjee, J. Lee, A. Rangarajan, L. Wan, N. Vidal, Q. Liu, A. Gainaru, N. Podhorszki, R. Archibald, S. Ranka, and S. Klasky. MGARD: A multigrid framework for high-performance, error-controlled data compression and refactoring. *SoftwareX*, 24:101590, 2023. doi: 10.1016/j.softx.2023.101590 3
- [19] A. Gyulassy, M. Duchaineau, V. Natarajan, V. Pascucci, E. Bringa, A. Higginbotham, and B. Hamann. Topologically clean distance fields. *IEEE Transactions on Visualization and Computer Graphics*, 13(6):1432–1439, 2007. doi: 10.1109/TVCG.2007.70603 1
- [20] D. Günther, R. A. Boto, J. Contreras-Garcia, J.-P. Piquemal, and J. Tierny. Characterizing molecular interactions in chemical systems. *IEEE Transactions on Visualization and Computer Graphics*, 20(12):2476–2485, 2014. doi: 10.1109/TVCG.2014.2346403 1
- [21] H. King, K. Knudson, and N. Mramor. Generating Discrete Morse Functions from Point Data. *Experimental Mathematics*, 14(4):435 – 444, 2005. 3, 4
- [22] S. Lakshminarayanan, N. Shah, S. Ethier, S. Klasky, R. Latham, R. Ross, and N. F. Samatova. Compressing the incompressible with ISABELA: In-situ reduction of spatio-temporal data. In *Proceedings of the 17th International Conference on Parallel Processing - Volume Part I*, Euro-Par'11, 14 pages, pp. 366–379, 2011. 3
- [23] F. Lan, B. Gamelin, L. Yan, J. Wang, B. Wang, and H. Guo. Topological characterization and uncertainty visualization of atmospheric rivers. *Computer Graphics Forum*, 43(3):e15084, 2024. doi: 10.1111/cgf.15084 2
- [24] T. Lewiner, H. Lopes, and G. Tavares. Optimal discrete Morse functions for 2-manifolds. *Computational Geometry*, 26(3):221–233, 2003. doi: 10.1016/S0925-7721(03)00014-2 3
- [25] Y. Li, X. Liang, B. Wang, Y. Qiu, L. Yan, and H. Guo. MSz: An efficient parallel algorithm for correcting Morse-Smale segmentations in error-bounded lossy compressors, 2024. 1, 2, 3, 4, 6, 7
- [26] X. Liang, S. Di, F. Cappello, M. Raj, C. Liu, K. Ono, Z. Chen, T. Peterka, and H. Guo. Toward feature-preserving vector field compression. *IEEE Transactions on Visualization and Computer Graphics*, 29(12):5434–5450, 2023. doi: 10.1109/TVCG.2022.3214821 3
- [27] X. Liang, S. Di, D. Tao, S. Li, S. Li, H. Guo, Z. Chen, and F. Cappello. Error-controlled lossy compression optimized for high compression ratios of scientific datasets. In *Proceedings of 2018 IEEE International Conference on Big Data*, pp. 438–447, 2018. doi: 10.1109/BigData.2018.8622520 1, 3
- [28] X. Liang, H. Guo, S. Di, F. Cappello, M. Raj, C. Liu, K. Ono, Z. Chen, and T. Peterka. Toward feature-preserving 2D and 3D vector field compression. In *Proceedings of 2020 IEEE Pacific Visualization Symposium*, pp. 81–90, 2020. doi: 10.1109/PacificVis48177.2020.9431 1
- [29] X. Liang, H. Guo, S. Di, F. Cappello, M. Raj, C. Liu, K. Ono, Z. Chen, and T. Peterka. Toward feature-preserving 2D and 3D vector field compression. In *Proceedings of 2020 IEEE Pacific Visualization Symposium*, pp. 81–90, 2020. doi: 10.1109/PacificVis48177.2020.9431 3
- [30] X. Liang, K. Zhao, S. Di, S. Li, R. Underwood, A. M. Gok, J. Tian, J. Deng, J. C. Calhoun, D. Tao, Z. Chen, and F. Cappello. SZ3: A modular framework for composing prediction-based error-bounded lossy compressors. *IEEE Transactions on Big Data*, 9(2):485–498, 2023. doi: 10.1109/TBDA.2022.3201176 1, 3
- [31] P. Lindstrom. Fixed-rate compressed floating-point arrays. *IEEE Transactions on Visualization and Computer Graphics*, 20(12):2674–2683, 2014. doi: 10.1109/TVCG.2014.2346458 1, 3
- [32] P. Lindstrom and M. Isenburg. Fast and efficient compression of floating-point data. *IEEE Transactions on Visualization and Computer Graphics*, 12(5):1245–1250, 2006. doi: 10.1109/TVCG.2006.143 1, 3
- [33] J. Liu, S. Di, K. Zhao, S. Jin, D. Tao, X. Liang, Z. Chen, and F. Cappello. Exploring autoencoder-based error-bounded compression for scientific data. In *Proceedings of 2021 IEEE International Conference on Cluster Computing (CLUSTER)*, pp. 294–306, 2021. doi: 10.1109/Cluster48925.2021.00034 3

- [34] R. G. C. Maack, J. Lukasczyk, J. Tierny, H. Hagen, R. Maciejewski, and C. Garth. Parallel computation of piecewise linear Morse-Smale segmentations. *IEEE Transactions on Visualization and Computer Graphics*, 30(4):1942–1955, 2024. doi: [10.1109/TVCG.2023.3261981](https://doi.org/10.1109/TVCG.2023.3261981) 9
- [35] M. Mrozek and T. Wanner. Coreduction homology algorithm for inclusions and persistent homology. *Computers & Mathematics with Applications*, 60(10):2812–2833, 2010. doi: [10.1016/j.camwa.2010.09.036](https://doi.org/10.1016/j.camwa.2010.09.036) 3
- [36] A. Otero-de-la Roza. Finding critical points and reconstruction of electron densities on grids. *The Journal of Chemical Physics*, 156(22):224116, 2022. doi: [10.1063/5.0090232](https://doi.org/10.1063/5.0090232) 2
- [37] S. Petruzza, A. Gyulassy, S. Leventhal, J. J. Baglino, M. Czabaj, A. D. Spear, and V. Pascucci. High-throughput feature extraction for measuring attributes of deforming open-cell foams. *IEEE Transactions on Visualization and Computer Graphics*, 26(1):140–150, 2020. doi: [10.1109/TVCG.2019.2934620](https://doi.org/10.1109/TVCG.2019.2934620) 1
- [38] V. Robins, P. J. Wood, and A. P. Sheppard. Theory and algorithms for constructing discrete Morse complexes from grayscale digital images. *IEEE Transactions on Pattern Analysis and Machine Intelligence*, 33(8):1646–1658, 2011. doi: [10.1109/TPAMI.2011.95](https://doi.org/10.1109/TPAMI.2011.95) 3
- [39] N. Shivashankar and V. Natarajan. Parallel computation of 3d Morse-Smale complexes. *Computer Graphics Forum*, 31(3pt1):965–974, 2012. doi: [10.1111/j.1467-8659.2012.03089.x](https://doi.org/10.1111/j.1467-8659.2012.03089.x) 2, 3, 4, 7, 9
- [40] N. Shivashankar, P. Pranav, V. Natarajan, R. v. d. Weygaert, E. P. Bos, and S. Rieder. Felix: A topology based framework for visual exploration of cosmic filaments. *IEEE Transactions on Visualization and Computer Graphics*, 22(6):1745–1759, 2016. doi: [10.1109/TVCG.2015.2452919](https://doi.org/10.1109/TVCG.2015.2452919) 1
- [41] M. Soler, M. Plainchault, B. Conche, and J. Tierny. Topologically controlled lossy compression. In *Proceedings of 2018 IEEE Pacific Visualization Symposium*, pp. 46–55, 2018. doi: [10.1109/PacificVis.2018.00015](https://doi.org/10.1109/PacificVis.2018.00015) 3
- [42] T. Sousbie. The persistent cosmic web and its filamentary structure - I. Theory and implementation. *Monthly Notices of the Royal Astronomical Society*, 414(1):350–383, 2011. doi: [10.1111/j.1365-2966.2011.18394.x](https://doi.org/10.1111/j.1365-2966.2011.18394.x) 1
- [43] D. Tao, S. Di, Z. Chen, and F. Cappello. Significantly improving lossy compression for scientific data sets based on multidimensional prediction and error-controlled quantization. In *Proceedings of 2017 IEEE International Parallel and Distributed Processing Symposium*, pp. 1129–1139, 2017. doi: [10.1109/IPDPS.2017.115](https://doi.org/10.1109/IPDPS.2017.115) 1, 3
- [44] Y. Xie, T. Takikawa, S. Saito, O. Litany, S. Yan, N. Khan, F. Tombari, J. Tompkin, V. Sitzmann, and S. Sridhar. Neural Fields in Visual Computing and Beyond. *Computer Graphics Forum*, 2022. doi: [10.1111/cgf.14505](https://doi.org/10.1111/cgf.14505) 3
- [45] L. Yan, X. Liang, H. Guo, and B. Wang. TopoSZ: Preserving topology in error-bounded lossy compression. *IEEE Transactions on Visualization and Computer Graphics*, 30(1):1302–1312, 2024. doi: [10.1109/TVCG.2023.3326920](https://doi.org/10.1109/TVCG.2023.3326920) 1, 3
- [46] K. Zhao, S. Di, M. Dmitriev, T.-L. D. Tonello, Z. Chen, and F. Cappello. Optimizing error-bounded lossy compression for scientific data by dynamic spline interpolation. In *Proceedings of ICDE'21: Proceedings of 2021 IEEE 37th International Conference on Data Engineering*, pp. 1643–1654, 2021. doi: [10.1109/ICDE51399.2021.00145](https://doi.org/10.1109/ICDE51399.2021.00145) 1, 3
- [47] K. Zhao, S. Di, X. Liang, S. Li, D. Tao, Z. Chen, and F. Cappello. Significantly improving lossy compression for HPC datasets with second-order prediction and parameter optimization. In *Proceedings of HPDC'20: Proceedings of the 29th International Symposium on High-Performance Parallel and Distributed Computing*, 12 pages, pp. 89–100, 2020. doi: [10.1145/3369583.3392688](https://doi.org/10.1145/3369583.3392688) 1, 3